Anal. Chem. **2009,** *81,* 5663–5670

Focused Ion Beam Fabrication of Boron-Doped Diamond Ultramicroelectrodes

Jingping Hu,[†] Katherine B. Holt,[‡] and John S. Foord*,[†]

Chemistry Research Laboratory, University of Oxford, Mansfield Road, Oxford OX1 3TA, United Kingdom, and Department of Chemistry, University College London, 20 Gordon Street, London WC1H 0AJ, United Kingdom

The fabrication of ultramicroelectrodes (UMEs) for analytical electrochemical applications has been explored, using boron-doped diamond as the active electrode material in an insulating coating formed by deposition of electrophoretic paint. Because of the rough nature of the diamond film, the property of such coatings that is normally exploited in the fabrication of UMEs, namely the tendency to retract automatically from sharp protrusions, cannot be used in the present instance. Instead focused ion beam (FIB) sputtering was employed to controllably produce UMEs with well-defined geometry, critical dimension of a few micrometers, and very thin insulating coatings. If the FIB machining is carried out at normal incidence to the diamond electrode surface, significant ion beam damage reduces the yield of successful electrodes. However, if a parallel machining geometry is employed, high yields of ultramicroelectrodes with a flat disk geometry can be obtained very reliably. The electrochemical properties of diamond UMEs are characterized. They show much lower background currents than the equivalent Pt or carbon fiber electrodes but more varied electrochemical response than macroscopic diamond electrodes.

Ultramicroelectrodes (UMEs) are electrodes with a critical size dimension below 25 μm and they have a crucial role in analytical electrochemistry, since they can offer significant advantages compared to macroscopic electrodes in many electrochemical applications.[1] Fast radial diffusion dominates the mass transport at the electrode surface, leading to enhanced detection sensitivity in electrochemical sensing and the ability to probe fast electron transfer kinetics. The small current drawn minimizes ohmic drop, enabling use in resistive media; the small electrode dimensions also enables the spatial dependence of the electrochemical signal to be exploited, in areas such as neurophysiology[2−4] and scanning electrochemical microscopy (SECM).[5] A typical ultramicroelectrode configuration consists of a conductive core (the electrode) surrounded by an insulating sheath, with an aperture in the insulator at the end of the electrode permitting contact with the solution. A well-defined geometry in this region of the probe is desirable, and a flat disk geometry is often preferred. In applications such as SECM, the electrode structure is often characterized by the ratio of insulation radius compared to the electrode disk radius (RG ratio) and this ideally should be as small as possible.[5]

Boron-doped diamond (BDD) has been used for electrodes in electrochemistry due to its unique combination of superior properties, including mechanical stability, chemical inertness, low background currents, wide potential window, and resistance to electrode fouling.[6] The applications of BDD for UMEs have been reported by several groups. Early work was reported by Cooper et al., by sealing diamond-coated tungsten wires in glass capillary and exposing the tip by polishing or etching in HF.[7] The RG ratio of the UME was large due to the thick wall of glass capillary, and the diamond electrode protruded from glass insulation as a result of polishing or etching, yielding diamond UMEs of effective diameter 6−14 μm. Fujishima et al. sandwiched a free-standing diamond film between two glass slides and polished the sandwich structure to expose an electrode area of 300 μm × 50 μm. The constructed band microelectrode was demonstrated in capillary electrophoresis analysis.[8] Swain and co-workers demonstrated various methods to construct diamond UMEs, including insulating the apex with polyimide film and exposing the apex by dissolving in sodium hydroxide or insulating the BDD tips with heat shrink tubing for application in capillary electrophoresis[9−11] The UMEs are in cylinder or conical geometry of typical 70 μm diameter with thick insulation layers. We recently reported the fabrication of BDD UMEs of small RG ratio and critical dimension of 1−25 μm and demonstrated the first applications of BDD UME in SECM.[12,13] The UME probes were first insulated with nitrocellulose and the tip apex was exposed by gently contacting it with filter paper

* Corresponding author. E-mail: john.foord@chem.ox.ac.uk.
[†] University of Oxford.
[‡] University College London.

(1) Heinze, J. *Angew. Chem., Int. Ed.* **1993**, *32*, 1268–1288.
(2) Qiao, Y.; Chen, J.; Guo, X. L.; Cantrell, D.; Ruoff, R.; Troy, J. *Nanotechnology* **2005**, *16*, 1598–1602.
(3) Soh, K. L.; Kang, W. P.; Davidson, J. L.; Wong, Y. M.; Cliffel, D. E.; Swain, G. M. *Diamond Relat. Mater.* **2008**, *17*, 900–905.
(4) Zoski, C. Z. *Electroanalysis* **2002**, *14*, 1041–1051.
(5) Bard, A. J.; Mirkin, M. V. *Scanning Electrochemical Microscopy*; Marcel Dekker: New York, 2001.
(6) Compton, R. G.; Foord, J. S.; Marken, F. *Electroanalysis* **2003**, *15*, 1349–1363.
(7) Cooper, J. B.; Pang, S.; Albin, S.; Zheng, J. L.; Johnson, R. M. *Anal. Chem.* **1998**, *70*, 464–467.
(8) Shin, D. C.; Sarada, B. V.; Tryk, D. A.; Fujishima, A. *Anal. Chem.* **2003**, *75*, 530–534.
(9) Cvacka, J.; Quaiserova, V.; Park, J.; Show, Y.; Muck, A.; Swain, G. M. *Anal. Chem.* **2003**, *75*, 2678–2687.
(10) Park, J.; Quaiserova-Mocko, V.; Peckova, K.; Galligan, J. J.; Fink, G. D.; Swain, G. M. *Diamond Relat. Mater.* **2006**, *15*, 761–772.
(11) Park, J.; Show, Y.; Quaiserova, V.; Galligan, J. J.; Fink, G. D.; Swain, G. M. *J. Electroanal. Chem.* **2005**, *583*, 56–68.
(12) Holt, K. B.; Caruana, D. J.; Raja, J.; Hu, J.; Foord, J. S. *ECS Trans.* **2007**, *3*, 37–47.
(13) Holt, K. B.; Hu, J. P.; Foord, J. S. *Anal. Chem.* **2007**, *79*, 2556–2561.

10.1021/ac9003908 CCC: $40.75
Published on Web 06/22/2009

soaked with acetone or else completely insulated with electrophoretic paint or fast set epoxy followed by polishing with 0.05 μm alumina or by contacting with acetone-soaked filter paper.

One of the notable methods to obtain low RG values is by insulating with electrophoretic paint, which can yield a thin layer coating with effective insulation.[14−17] Electrophoretic paint was first commercialized by Ford Motor Co. for the car industry[18] and is commercially available. The cathodic paint consists of positively charged micelles dispersed in aqueous media, which precipitate on the electrode surface as a thin, uniform, and tightly adherent polymer film when a negative electrode potential is applied to it, due to a local pH rise as a result of water hydrolysis. This polymer film is transformed to an electrically insulating and relatively chemically inert layer upon curing. It was discovered that the paint shrinks and retracts during curing and leaves a sharp conductive tip exposed if a sharp needle-shaped substrate is employed.[15] These properties of electrophoretic paint have been taken advantage of in the fabrication of STM tips[19,20] and Pt, W, Au, or carbon fiber UMEs.[14,16,17] We have tried to exploit the tip retraction properties of electrophoretic paint in the fabrication of diamond UMEs, but it only works rarely. (The reason why electrophoretic paint failed to expose BDD UMEs will be discussed later in this paper.) It nevertheless provides an excellent means to prepare fully insulated diamond tip electrodes, but then some method is needed to remove the paint from the tip itself, to allow contact with the electrochemical medium.

Developing a method to expose the apex of electrodes after insulation is always a challenge in the fabrication of UMEs. Polishing, etching, and cutting have been reported, and the methods we have used previously[12,13] generally do not yield a good electrode with well-defined and flat disk geometry suitable for SECM, and the electrode size is also hard to control. Focused ion beam (FIB) is a well-established micromachining tool for a wide range of applications, such as TEM sample preparation, nanostructure production, and IC circuit modification.[21] Qiao et al. demonstrated the fabrication of tungsten nanoelectrodes for neurophysiology applications by electrophoretic paint insulation and FIB milling.[2] Arrigan and co-workers reported the fabrication of nanopore arrays by milling pores through silicon nitride insulating layer above the Pt plane electrode.[22] Macpherson et al. fabricated a SWNT UME for SECM-AFM applications.[23] Despite the activities of FIB in the fabrication of metal and SWNT UMEs, the authors are not aware of the use of FIB in the fabrication of BDD UMEs. Unlike metals or SWNT, the electrochemical properties of BDD electrodes are more vulnerable to modification by the incidence of high energetic ion beam,[24,25] which make the application of FIB in BDD UME fabrication quite different from that of other materials.

In this paper, we demonstrate a novel approach to fabricate BDD UMEs suitable for SECM applications by FIB, explore the influence of FIB conditions on the performance of the electrodes, and demonstrate the superior electrochemical characteristic of BDD UMEs over platinum and carbon fiber UMEs.

EXPERIMENTAL SECTION

Materials and Chemicals. Tungsten wire of 250 μm diameter was obtained from Goodfellow (Cambridge, UK). Cathodic electrophoretic paint was obtained from ANCA Electrocoat Ltd. (Warwick, UK). Hexaammineruthenium [$Ru(NH_3)_6^{3+}$] trichloride (98%), ferrocene methanol (FcOH, 97%), and potassium hexachloroiridate(IV) ($IrCl_6^{2-}$, 99.99%) were obtained from Aldrich and used as redox couples without further purification. The supporting electrolytes were 1.0 M acetate buffer solution for $Ru(NH_3)_6^{3+}$ and 0.5 M KCl for the other compounds. All solutions were prepared with Milli-Q water (>18 MΩ cm).

Growth of Diamond Film and UME Preparation. The tungsten wire was electrochemically etched to a needle profile in 2 M NaOH using a dc voltage. After etching it was rinsed with copious amounts of Milli-Q water and ultrasonically seeded in nanodiamond powder (3 nm diameter, Bio York Ltd., UK) suspensions for 30 min. The seeded tungsten tips were mounted 4 mm below a tungsten filament in a hot-filament-assisted chemical vapor deposition (HFCVD) chamber that was fed with a mixture of 0.7% methane in hydrogen gases at a total flow rate of 160 sccm. The W wire tips are pointed toward the hot filament in the CVD reactor; they are heated both by the hot gases/radiation from the spiral filament and also from a heated substrate holder. This maintains the temperature over the W tip within the diamond growth "window" to get uniform coating. Boron doping was introduced by bubbling the hydrogen through an ice-cooled bubbler containing trimethylborate (99%, Aldrich). A negative electrical bias of −60 V was applied throughout the growth to improve the diamond morphology, and full details of the optimal growth conditions for this application are discussed elsewhere.[26]

The diamond-coated tungsten needles were insulated with cathodic electrophoretic paint for insulation. The diamond electrode was used as cathode and a platinum coil was used as anode. The coating was deposited at 5 V bias for 1 min, followed by rinsing with copious amounts of water to remove excess paint. The insulated electrode was secured vertically with sharpened tips upward in an oven and cured at 180 °C for 30 min. This deposition and curing process was repeated for many cycles to make sure that the coating was free of pinholes, as judged by the absence of a Faradaic current in electrochemical experiments using the insulated electrodes.

The apex of the insulated diamond needles was milled in a focused ion beam facility (FEI 200), equipped with a liquid gallium ion source. The acceleration voltage was 30 kV, operated at a spot size of 10 nm. A low beam current (1 or 10 pA) to carry out a

(14) Chen, S. L.; Kucernak, A. *Electrochem. Commun.* **2002**, *4*, 80–85.
(15) Schulte, A.; Chow, R. H. *Anal. Chem.* **1996**, *68*, 3054–3058.
(16) Slevin, C. J.; Gray, N. J.; Macpherson, J. V.; Webb, M. A.; Unwin, P. R. *Electrochem. Commun.* **1999**, *1*, 282–288.
(17) Zhu, L.; Claude-Montigny, B.; Gattrell, M. *Appl. Surf. Sci.* **2005**, *252*, 1833–1845.
(18) Fisher, T. P.; Fisher, C. *Surf. Technol.* **1981**, *12*, 107–125.
(19) Bach, C. E.; Nichols, R. J.; Meyer, H.; Besenhard, J. O. *Surf. Coatings Technol.* **1994**, *67*, 139–144.
(20) Mao, B. W.; Ye, J. H.; Zhuo, X. D.; Mu, J. Q.; Fen, Z. D.; Tian, Z. W. *Ultramicroscopy* **1992**, *42*, 464–467.
(21) Volkert, C. A.; Minor, A. M. *MRS Bull.* **2007**, *32*, 389–395.
(22) Lanyon, Y. H.; De Marzi, G.; Watson, Y. E.; Quinn, A. J.; Gleeson, J. P.; Redmond, G.; Arrigan, D. W. M. *Anal. Chem.* **2007**, *79*, 3048–3055.
(23) Burt, D. P.; Wilson, N. R.; Weaver, J. M. R.; Dobson, P. S.; Macpherson, J. V. *Nano Lett.* **2005**, *5*, 639–643.
(24) Foord, J. S.; Goeting, C. H. *Phys. Status Solidi A* **2004**, *201*, 2439–2443.
(25) Kondo, T.; Ito, H.; Kusakabe, K.; Ohkawa, K.; Einaga, Y.; Fujishima, A.; Kawai, T. *Electrochim. Acta* **2007**, *52*, 3841–3848.
(26) Hu, J. P.; Foord, J. S.; Holt, K. B. *Phys. Chem. Chem. Phys.* **2007**, *9*, 5469–5475.

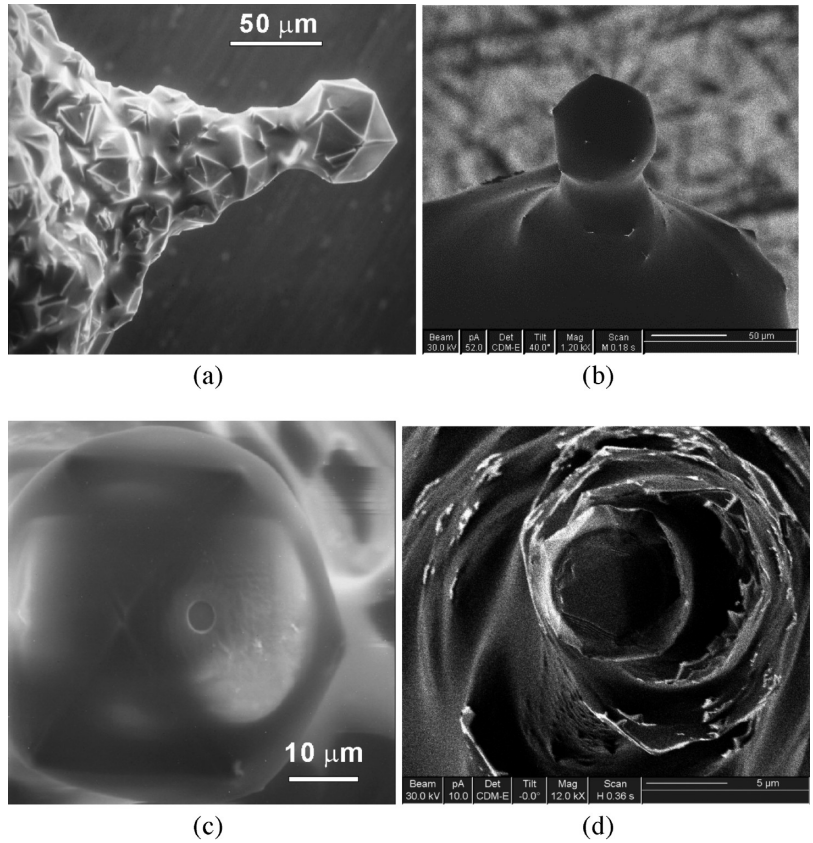

Figure 1. SEM and FIB images of (a) a single crystal BDD electrode insulated with a thinner layer of electrophoretic paint, the same electrode (b) with thicker insulation, and (c) after head-on milling with FIB. (d) FIB image of BDD UME after head-on FIB milling, with underlying diamond grain exposed and discernible.

single scan with fast scan rates was used for focusing and imaging to minimize the undesired exposure of the insulation layer; medium beam currents (100−500 pA) were employed for ion milling. The sputtering rate of electrophoretic paint and BDD was calibrated relative to silicon.

Physical and Electrochemical Characterization. The surface morphology was characterized by scanning electron microscopy (SEM, Hitachi S200) with a thermal emission electron source and 20 kV acceleration voltages. Raman spectra were acquired by Renishaw InVia Raman microscope with Ar^+ laser (514.5 nm). Raman spectra were taken with 50× microscope objective and the laser-focused area was about 1 μm in diameter.

Electrochemical measurements were carried out at 20 ± 2 °C with an Autolab PSTAT10 with a standard three-electrode cell, comprising a platinum counter electrode and a standard calomel (SCE) or Ag/AgCl reference electrode. The cell was housed in an electrically grounded Faraday cage to eliminate external electrical noise and enhance the signal/noise ratio. A 2 μm diameter platinum UME (fabricated by sealing Pt Wallaston wire in glass after acid stripping of the Ag coating) and a 7 μm diameter carbon fiber UME (BAS Inc.) were used for comparison with the "in-house" BDD UMEs. Both the C-fiber and Pt microelectrode were pretreated using the same procedure: both were polished using 0.3 μm alumina powder suspension and a soft cloth and rinsed with deionized water. As-grown or H-plasma-treated diamond electrodes are H-terminated, if subject to limited use in a narrow potential window (see ref 6 and references therein). However, in view of the processing steps used to produce the final diamond UMEs in the present work, and also because of the fact that the results reported were observed from electrodes that were used extensively, we anticipate that the diamond electrodes described will be predominantly terminated with oxygen functional groups. The electrodes were rinsed with deionized water prior to use.

RESULTS

The sharpened tungsten wire was first coated with a conformal layer of BDD. Depending on the growth conditions, polycrystalline diamond electrodes can be achieved, but sometimes single crystalline (Figure 1a) forms are exposed at the tip. The diamond electrodes were insulated by electrophoretic paint. Figure 1a shows the SEM image of single crystal diamond electrode with a thin layer of paint. For most of the samples we failed to obtain a satisfactory working UME from the shrinking and retraction of electrophoretic paint during curing. Instead conductive regions were found distributed along the length of the electrode, presumably because the paint retracts from the sharp diamond grain edges, which comprise the diamond coating. So many paint deposition−curing cycles were employed to ensure that the UME was insulated completely, as can be seen in Figure 1b, where no diamond grains are discernible and the ultramicroelectrode looks completely dark. Cross-sectional imaging suggests the paint insulation layer is around 0.1 μm thick for this extensive deposition.

The apexes of insulated BDD UMEs were exposed by FIB milling in two types of geometry, in order to open up an aperture

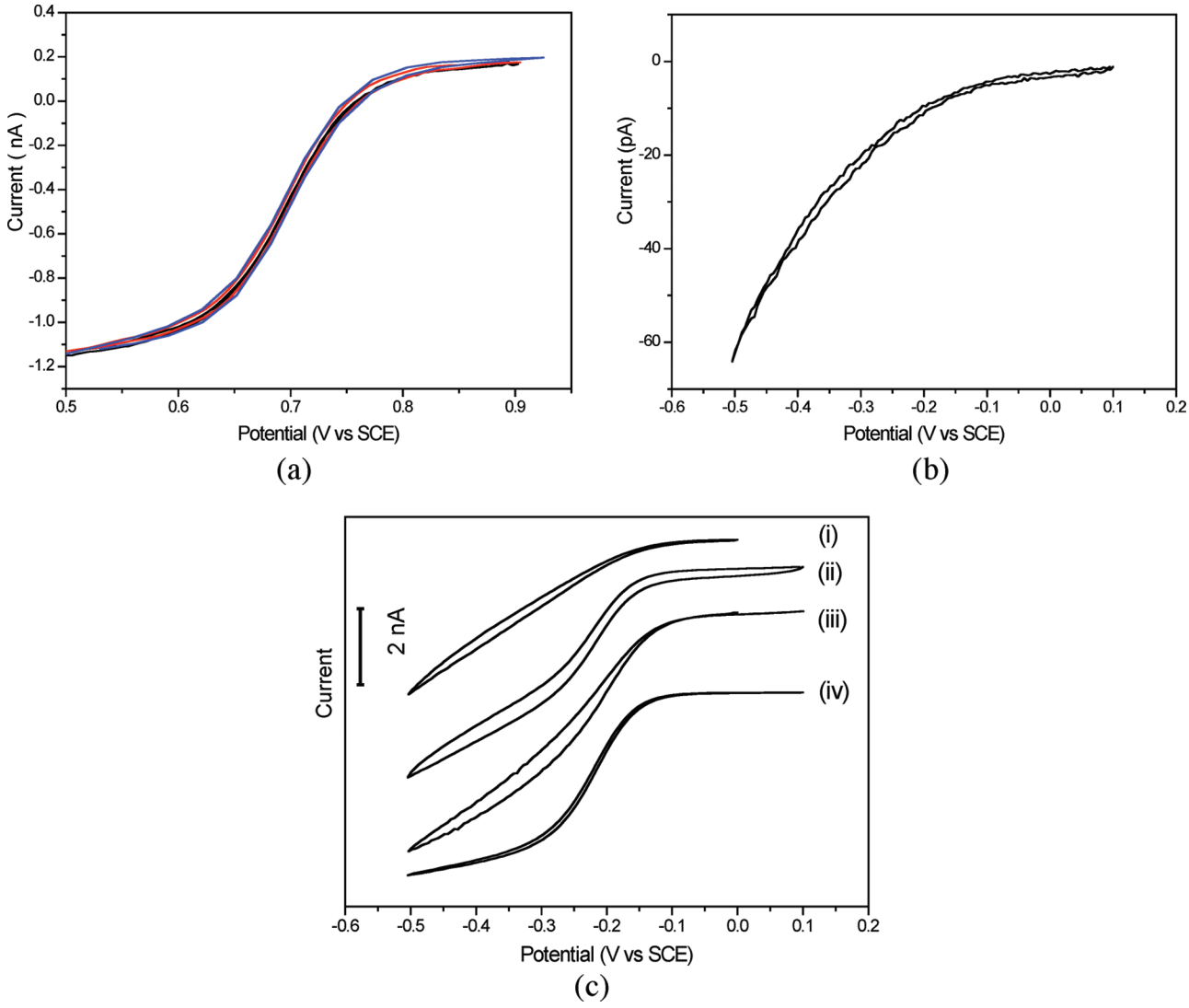

Figure 2. Cyclic voltammetry of (a) the same BDD UME as Figure 1c, measured with scan rates of 10, 100, 250 mV/s in 1 mM $IrCl_6^{2-}$; (b) the same UME as Figure 1d, measured in 1 mM $Ru(NH_3)_6^{3+}$; (c) a series of UMEs fabricated from different sample orientations relative to ion beam, measured in 1 mM $Ru(NH_3)_6^{3+}$, (i) head-on, (ii) 30° from head-on, (iii) 60° from head-on, and (iv) side-on ion milling.

in the insulating electrophoretic paint layer: "head-on", where the ion beam is directly incident in a perpendicular geometry onto the diamond surface, and "side-on", where the ion beam is parallel to the exposed electrode surface. Figure 1c shows an SEM image of the same electrode in Figure 1b after head-on milling in the center of apex by the ion beam, using a beam current of 100 pA for 6 min. The milled pattern is a circle of 3 μm diameter, and the depth is around 0.3 μm, which is thicker than the thickness of the paint to make sure the diamond electrode is exposed.

The electrochemical performance was assessed by cyclic voltammetry (CV) in 1 mM $IrCl_6^{2-}$, as presented in Figure 2a. The voltammogram shows a sigmoidal curve, typical of microelectrodes, with steady state current $I_{lim} = 1.2$ nA. The effective electrode diameter can be calculated from the equation $I_{lim} = 5.14nFDCr$ assuming a disk geometry and a small RG ratio of 1.1.[5] In this equation, n is the number of electrons transferred per molecule in the electrochemical reaction, F is the Faraday constant, D is the diffusion coefficient, C is the concentration of redox active species, and r is the radius of the disk electrode. The diffusion coefficient of 7.5×10^{-6} cm^2/s is used for $IrCl_6^{2-}$,[27,28] and the calculated UME diameter is 3.23 μm. This value is reasonably consistent with the diameter of 3 μm measured directly from the SEM image. The CV measurement was repeated with different scan rates in the range 25−250 mV s^{-1}, and all of them overlap quite well, demonstrating a "steady state" response due to radial diffusion. The Tomes criterion ($E_{3/4} - E_{1/4}$) was calculated to be 57.1 mV, which is consistent with the theoretical value of 56 mV.[29] The smallest BDD UME we achieved using this approach shows a limiting current of 0.9 nA in 1 mM $Ru(NH_3)_6^{3+}$, corresponding to a radius of 2 μm assuming a RG ratio of 1.1 and a disk geometry.

FIB milling with a head-on geometry did not always produce a UME showing sigmoidal electrochemical responses as illustrated above. Of the 30 BDD electrodes we processed using this approach, less than a third exhibited satisfactory electrochemical behavior. Many UMEs showed very poor electrochemical re-

(27) Beriet, C.; Pletcher, D. *J. Electroanal. Chem.* **1994**, *375*, 213–218.
(28) Macpherson, J. V.; Jones, C. E.; Unwin, P. R. *J. Phys. Chem. B* **1998**, *102*, 9891–9897.
(29) Tomes, J. *Collect. Czech. Chem. Commun.* **1937**, *9*, 81.

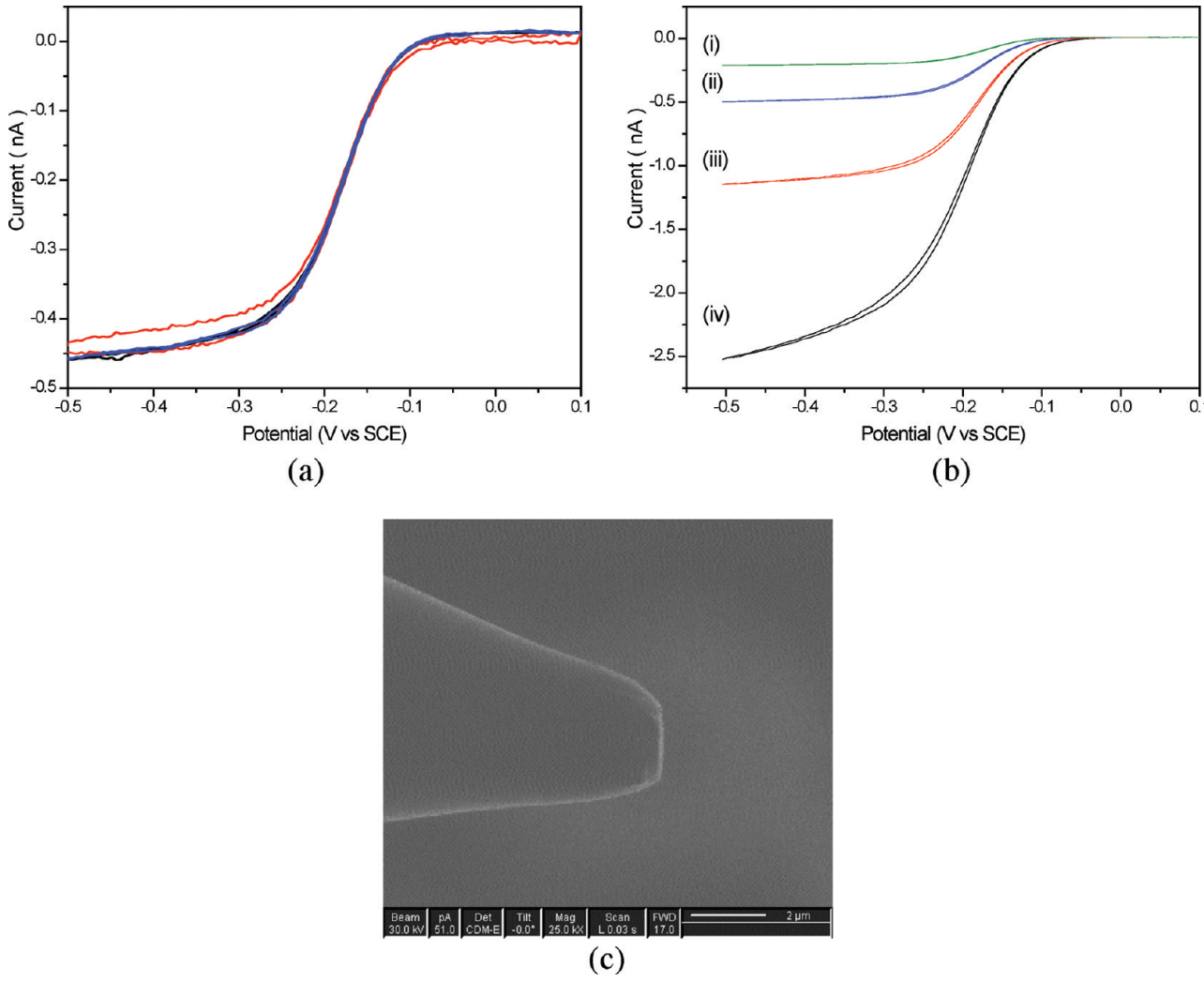

Figure 3. Cyclic voltammograms of the smallest diamond UME obtained from side-on FIB milling. (a) CV at different scan rates: black, 25 mV/s; red, 50 mV/s; blue, 100 mV/s. (b) CV in different concentrations of $Ru(NH_3)_6^{3+}$: (i) 0.5 mM, (ii) 1 mM, (iii) 2 mM, and (iv) 4 mM. (c) FIB image shows the radius <1 μm, fabricated from side-on ion milling.

sponse in the three redox mediators we tested, encompassing $Ru(NH_3)_6^{3+}$, FcOH, and $IrCl_6^{2-}$. Figure 2b shows a typical cyclic voltammogram of an UME that was milled by ion beam, in this case using a beam current of 554 pA for 2.3 min. The electrode was milled for a disk shape of 7 μm diameter and 0.3 μm depth and is illustrated by the SEM image in Figure 1d, where the texture of a single diamond grain can easily be seen. An ill-defined and nonsigmoidal current response is observed with no discernible limiting current, indicative of slow electron transfer kinetics toward $Ru(NH_3)_6^{3+}$ with a strong background current which increases steadily to negative potentials.

One problem is presumably associated with the fact that impact of the highly energetic incident ion beam with the diamond surface using the head-on configuration destroys the electrode surface, and this is discussed further in the Summarizing Remarks below. To explore the influence of electrode orientation relative to ion beam during milling, BDD UMEs were milled, starting from head-on position, tilting away to 30°, 60° from the head-on position, and finally flipping over to the side-on milling geometry. Figure 2c illustrates the different typical CVs for these electrodes in 1 mM $Ru(NH_3)_6^{3+}$. As the electrode tilts away from the head-on configuration, the electrochemical response improves gradually and finally gives a perfect sigmoidal curve at the side-on orientation.

Almost all the electrodes milled from the side-on configuration, which sputters away the entire end of the insulation and diamond structure to expose a disk electrode, exhibits excellent electrochemical performance. The diameter of achieved UME mainly depends on the sharpness of the electrode, and the smallest radius obtained is slightly less than 1 μm diameter (Figure 3c), which is consistent with the limiting current of 0.45 nA in 1 mM $Ru(NH_3)_6^{3+}$ if a RG value of 1.1 and a disk geometry is considered. CV was performed in $Ru(NH_3)_6^{3+}$ with scan rates from 25, 50, and 100 mV/s, as shown in Figure 3a, all of which superimposed each other quite well, demonstrating the steady state achieved on the UME surface, which is independent of scan rate. Figure 3b illustrates the CV responses in 0.5, 1, 2, and 4 mM $Ru(NH_3)_6^{3+}$ with scan rates of 50 mV/s. The limiting current is almost linear with concentration, which is consistent with theoretical predictions.

Raman spectroscopy was employed to characterize the crystalline structure modification of BDD ultramicroelectrodes milled

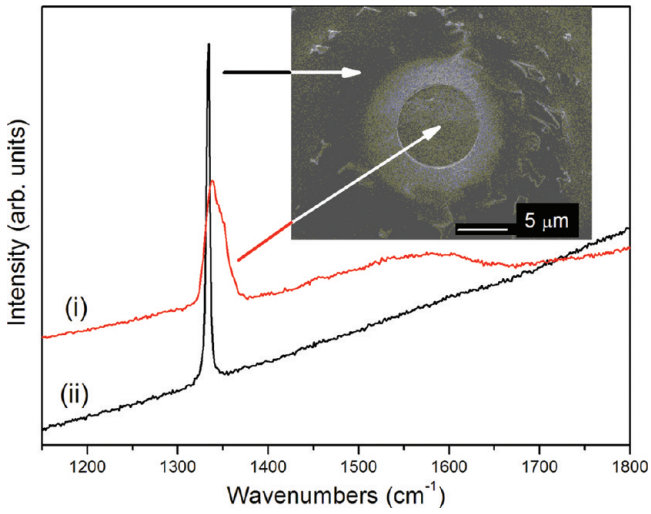

Figure 4. Typical Raman spectra measured from two areas on a head-on milled BDD UME, as indicated in the inset FIB figure, (i) inside the FIB area and (ii) outside the FIB area.

with various ion beam orientations. Figure 4 shows the Raman spectra of diamond UME fabricated from the head-on FIB milling. The electrode assessed here was first coated by polycrystalline BDD, followed by FIB milling with an ion beam flux of 111 pA, to produce a disk of 8 μm diameter and 0.4 μm milling depth. It exhibits poor electrochemical response in all three types of redox mediators studied. The Raman spectra were sampled from a few positions across the sample, as shown in the inset image of the Raman spectra. All the spectra sampled outside of the milled disk show very similar character, as do the spectra inside the disk. Typical spectra in both regions are shown in Figure 4i,ii.

The spectra from outside the region of FIB milling show a very sharp and well-defined peak at 1332 cm^{-1} which is a characteristic peak of diamond. In stark contrast, the Raman spectra inside the milling area exhibit overlapping of two broadened peaks at 1332 and 1345 cm^{-1}. The former is the diamond characteristic peak and the latter is the D-band of carbon peak, which is associated with sp^2 amorphous carbon. In addition, a broad peak ranging up to losses of 1580 cm^{-1} also appears, indicating the presence of amorphous carbon (the G band). The Raman spectra give direct evidence of the diamond phase modification by high energetic ion beam irradiation using the head-on machining geometry. In contrast, little change was visible in the Raman spectrum when a side-on geometry was used.

The BDD UMEs exhibited different CV behaviors in different electrochemical systems. Figure 5a illustrates the CVs of the same BDD UME in three different redox couple solutions. It has a single crystalline grain at the apex and is milled head-on to a depth of 0.6 μm with 1000 pA ion beam flux to get a disk of 8 μm diameter. It shows satisfactory electrochemical response in 1 mM $Ru(NH_3)_6^{3+}$, slight deteriorated response in 1 mM FcOH, and a significant decrease in electrochemical activity in 1 mM $IrCl_6^{2-}$. However, it is not always the case that BDD UMEs exhibit better performance in $Ru(NH_3)_6^{3+}$ than in FcOH, or better in FcOH than in $IrCl_6^{2-}$. This variation in response is further illustrated in Figure 5b for a different BDD UME which shows good CV performance in FcOH and was also found to respond well to $Ru(NH_3)_6^{3+}$. Figure 2a presents a sigmoidal CV in $IrCl_6^{2-}$ for the single crystal diamond UME shown in Figure 1a–c. However, despite the excellent response toward $IrCl_6^{2-}$, it shows a poor CV behavior in $Ru(NH_3)_6^{3+}$. Overall, it is quite noticeable that these diamond UMEs show much more variability in performance than macroscopic diamond electrodes.[6]

The electrochemical performances of BDD UMEs (4 μm diameter) produced by FIB milling were compared with those of conventional Pt UME (2 μm diameter) and carbon fiber UME (7 μm diameter). All of them show good CV behavior in 1 mM FcOH, as shown in Figure 6a, with limiting currents consistent with the electrode diameter. Figure 6b compares the background signal of these three types of UMEs in 0.1 M KCl solution where the current is normalized to the electrode area to obtain current density for comparison. Apparently, the BDD UME exhibits the lowest background current density. The current density is higher for the carbon fiber UME, presumably due to the high concentration of ionizable functional groups, which tend to be present on such electrodes and highest for platinum UME, where some

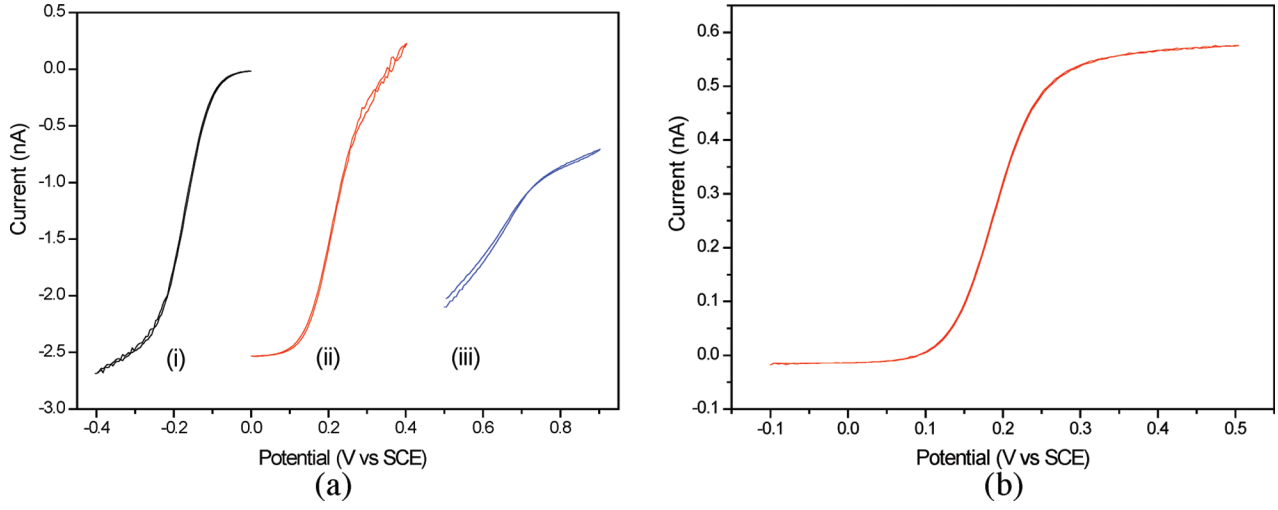

Figure 5. (a) Different CV response of the same diamond UME measured with different redox couples: (i) 1 mM $Ru(NH_3)_6^{3+}$, (ii) 1 mM FcOH, (iii) 1 mM $IrCl_6^{2+}$. (b) CV of another diamond UME that shows a reversible sigmoidal curve in 1 mM FcOH.

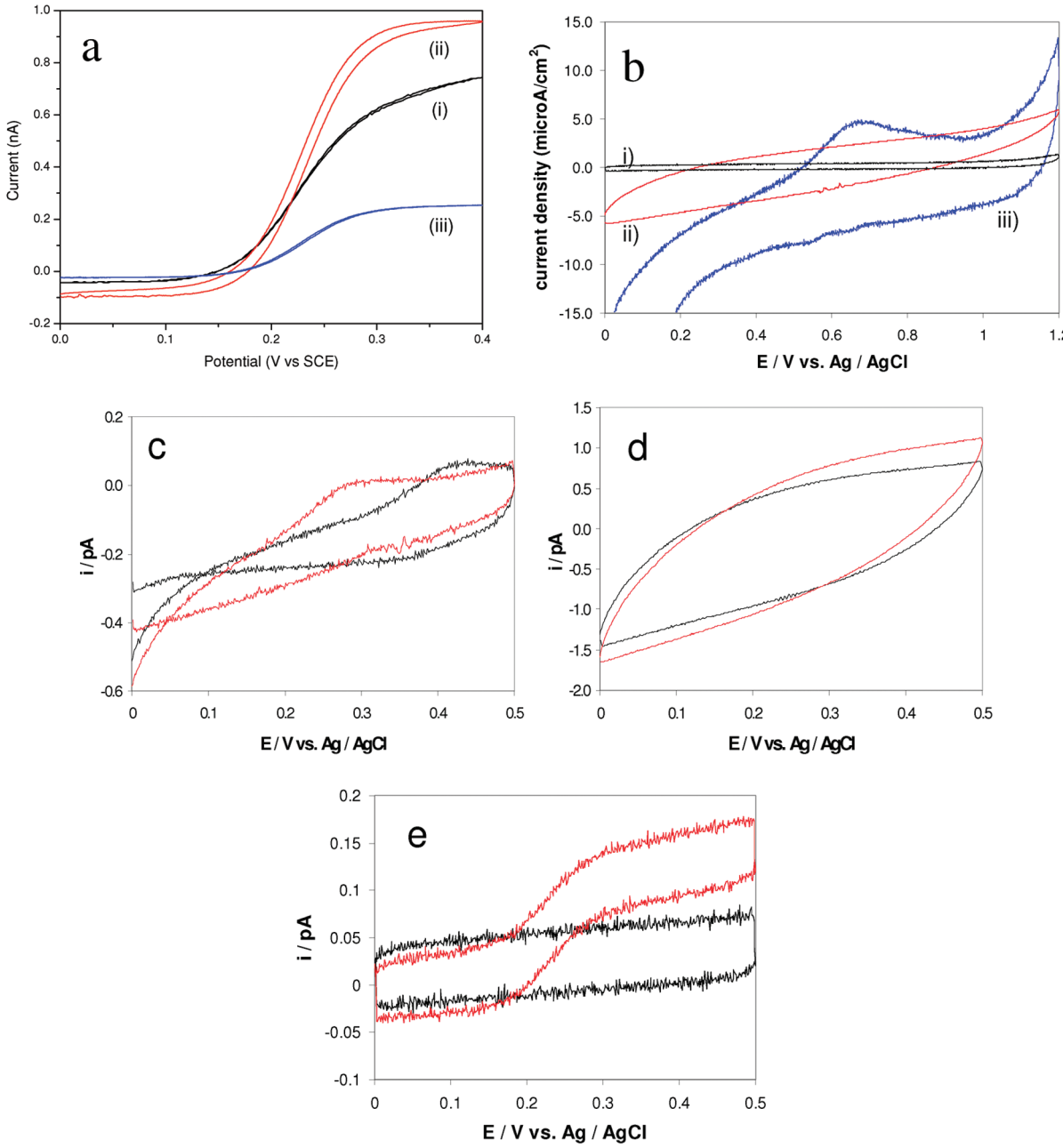

Figure 6. (a) CVs of the three UMEs exhibit reversible sigmoidal curve in 1 mM FcOH. (i) BDD UME of 4 μm diameter, (ii) carbon fiber UME of 7 μm diameter, and (iii) platinum UME of 2 μm diameter. (b) A comparison of the background CV curves of the three UMEs in 0.1 M KCl supporting electrolyte. Same labeling as part a. (c) CV of the Pt UME (iii) in 1 μM FcOH (red trace) compared to background (black trace). Part d is as for part c but for the carbon UME (ii). Part e is as for part c but for the diamond UME (i).

features observed associate with the formation of PtO_x^-. From the quantitative analysis it is estimated that the background current density of BDD UME is about 30 times smaller than that of the Pt UME background current density and about 5 times smaller than the C fiber UME background current density.

These three UMEs were employed to detect very dilute solutions containing 1 μM FcOH, as shown in Figure 6c−e. An obvious sigmoidal electrochemical response with a clear limiting current is discernible for the BDD UME in such dilute solutions. In contrast, the background signals for the carbon fiber and platinum UMEs rather overwhelm the expected faradaic response for FcOH.[10]

SUMMARIZING REMARKS

In this paper, we have developed a route for the fabrication of diamond UME structures based on the use of electrophoretic paints as the insulation medium. In the successful applications of electrophoretic paints for microelectrode fabrication reported previously, which exploit the ability of the coating to retract naturally from sharp tips, the substrates have been typically sharpened Pt−Ir, Pt, W, Au, or carbon fibers,[14,16,17] all of which bear a smooth surface due to electrochemical etching. For these substrates, the electrophoretic paint deposition is very thin in the vicinity of the tip apex and becomes thicker away from the apex. However, this is hard to realize for BDD tips, where the diamond coating blunts the tip and the big diamond grains make the sur-

face appear very rough. Although conformal, smooth, thin nanodiamond coatings might give a more favorable morphology for use with electrophoretic paints, we have shown elsewhere that such material does not display optimal electrochemical properties.[26] A better way, therefore, would appear to use thick insulating paint coatings but then exploit a controlled route to opening the insulation to allow electrolyte access to the diamond electrode.

We have shown this can be successfully achieved using FIB methods and have examined two machining geometries. Of the two electrode orientations used for FIB milling, almost 100% success rate can be achieved for side-on milling, but head-on milling is rather less successful, with less than a third showing good electrochemical properties. The deleterious impact of the high energetic incident ion beam on the specimen surface at normal incidence leads not only to removal of materials by sputtering process but the generation of defects or even amorphization that extends tens of nanometers into the materials.[21] Foord et al. reported the modification of diamond electrode by moderate energetic Ar^+ ion bombardment (10^{14} ions/cm^2 at 1000 V),[24] and the electrochemical kinetics of some redox couples are strongly inhibited on the treated BDD surface. FIB utilizes a much higher acceleration voltage (30 kV) and the ion intensity is also several orders magnitude higher, so it is not surprising that only a small portion of the electrodes are able to survive from the FIB at head-on milling configuration. It might have been expected that ion beam damage would serve to graphitize the electrode, improve conductivity, and therefore maintain a good electrochemical response. That the opposite is observed may have two origins. First, ion beam processing of carbon materials often tends to produce carbon forms such as diamond-like carbon or tetrahedral amorphous carbon, which have poor conductivity. Second, it is possible that the ion beam damage produces interfacial carbon forms that are either in poor contact with the underlying (conductive) diamond phase or which become very heavily oxidized when the electrode is exposed to air or the solution.

In contrast to the strong radiation damage during head-on milling, the damage by glancing incidence of FIB at the side-on position is significantly reduced due to minimum momentum transfer at this angle. Head-on milling gives the most flexibility with regard to the shape and size of electrode that can be achieved, but the side-on approach is fully viable and can be used routinely. It simply requires the additional condition that the end tip radius of the grown diamond-on tungsten structure is roughly similar in size to that of the required UME, which can be achieved by control of the CVD growth process. It results in very flat, disk-shaped UMEs, which is useful in applications such as SECM, since it enables the probe to approach closer to the substrate.

It was notable that the diamond UMEs showed quite variable response to the redox couples investigated. The majority of diamond electrodes used for electrochemical research are of macroscopic dimensions and by and large show reproducible behavior, typically fast "reversible" or "quasireversible" kinetics, for the couples studied here. However, localized measurements of such electrodes by techniques such as SECM, conductive AFM, Raman microscopy, and Kelvin probe microscopy show they are heterogeneous in activity across their area.[30−34] In particular, response toward different redox couples varied with location on the electrode surface.[33] Several factors are proposed to influence the heterogeneity of BDD electrodes, with the most obvious arising from the boron dopant incorporation during CVD growth. The electrodes are normally polycrystalline in nature, with the variable grain orientation leading to differing crystallographic faces being exposed at the growth interface, particularly (111) and (100) crystal orientations. Boron is more readily included into (111) facets than (100) sectors, leading to a concentration that varies spatially across the surface.[32,34] In addition, variations in work function, surface termination, fraction of sp^2-bonded carbon in the grain boundaries and defect sites, and the presence of adsorbates may also contribute to the heterogeneous activity.[32,33] For large area electrodes, spatial averaging leads to reproducible behavior. However, for very small diamond UMEs this is not the case. Further research will be necessary to understand and control the factors involved. However, it should be noted that it is definitely not connected to the milling process, since we also observe it on microelectrodes fabricated by other routes.[13]

Some of the excellent properties of diamond UMEs are shown in this work, where the much lower background current, as a result of smaller double layer capacitance and absence of interfering Faradaic contributions compared to carbon fiber and Pt UMEs, enables analytical signals at significantly lower concentrations to be recorded.

ACKNOWLEDGMENT

J.H. acknowledges Dr. Kerstin Jurkschat in the Materials Science Department of Oxford University for help with some of the FIB experiments and acknowledges the financial support of Newton Abraham studentship. K.B.H. acknowledges the Ramsay Trust and Kodak for a Ramsay Fellowship and the EPSRC for an Advanced Research Fellowship. This project was funded by EPSRC grant no. EP/D504813/1.

Received for review February 20, 2009. Accepted June 9, 2009.

AC9003908

(30) Colley, A. L.; Williams, C. G.; Johansson, U. D.; Newton, M. E.; Unwin, P. R.; Wilson, N. R.; Macpherson, J. V. *Anal. Chem.* **2006**, *78*, 2539–2548.
(31) Holt, K. B.; Bard, A. J.; Show, Y.; Swain, G. M. *J. Phys. Chem. B* **2004**, *108*, 15117–15127.
(32) Szunerits, S.; Mermoux, M.; Crisci, A.; Marcus, B.; Bouvier, P.; Delabouglise, D.; Petit, J. P.; Janel, S.; Boukherroub, R.; Tay, L. *J. Phys. Chem. B* **2006**, *110*, 23888–23897.
(33) Wang, S. H.; Swain, G. M. *J. Phys. Chem. C* **2007**, *111*, 3986–3995.
(34) Wilson, N. R.; Clewes, S. L.; Newton, M. E.; Unwin, P. R.; Macpherson, J. V. *J. Phys. Chem. B* **2006**, *110*, 5639–5646.